

Supporting Information

Zwitterionic Bifunctional Layer for Reversible Zn Anode

Renpeng Chen¹, Qin Liu¹, Lin Xu^{1,2}, Xuri Zuo¹, Fang Liu¹, Jianyong Zhang¹, Xuan Zhou¹, and Liqiang Mai^{1,2*}*

¹ State Key Laboratory of Advanced Technology for Materials Synthesis and Processing, School of Materials Science and Engineering, Wuhan University of Technology, Wuhan 430070, Hubei, P. R. China

² Foshan Xianhu Laboratory of the Advanced Energy Science and Technology Guangdong Laboratory, Xianhu Hydrogen Valley, Foshan 528200, Guangdong, P. R. China

Corresponding Author

*E-mail: linxu@whut.edu.cn (Lin Xu); mlq518@whut.edu.cn (Liqiang Mai);

Experimental section

Synthesis of 1-Vinyl-3-carboxylate-imidazol: 1-vinyl-3-carboxylate-imidazol was synthesized according to the previous work.¹ First, 7.05 g vinyl imidazole (99%, Aladdin) and 8.95 g methyl chloroacetate (AR, Aladdin) was stirred at room temperature for 2 days. Then the mixed precursor was washed 3 times with diethyl ether and dried under vacuum at 30 °C for 12 h, a white powder product was obtained. Second, 7 g white powder above and 2.14 g KOH into a solvent of ethanol (40 mL), stirring for 2 h. The crude product was separated by the centrifuge at a speed of 10000 r min⁻¹ for 3 min. Then the crude product was washed 3 times with ethanol and dried under vacuum at 30 °C for 12 h. Finally, 1-Vinyl-3-carboxylate-imidazol was obtained.

Preparation of PZIL-Zn electrodes: 1.2 g acrylamide and 0.64 g 1-vinyl-3-(carboxymethyl)-imidazole was added in 10ml deionized water while stirring until monomer dissolved. Then 18.4 mg ammonium persulfate (99.99%, Aladdin), 1 wt% N,N,N',N'-tetramethyl ethylenediamine (Aladdin), and 3 mg N,N-methylenebisacrylamide (99%, Aladdin) were added to the solutions above. To prepare PZIL-Zn, the as-prepared solution was coated on the surface of Zn plate by spin-coating under 3000 rpm for 15 s.

Synthesis of MnO₂/CNT: MnO₂/CNT nanocomposites were synthesized by a hydrothermal method reported in the previous literature.² Firstly, 1.13 g Mn(CH₃COO)₂·4H₂O (AR, Aladdin) was added to 50 mL of deionized water, then 0.16

g CNT was added into the solution under continuously stirring. Second, the above mixed solution was added slowly into 25 mL aqueous solution, which dissolved 1.45 g KMnO_4 (AR, Aladdin). Third, after stirring for 2 h, the mixed solution was transferred to a Teflon-lined autoclave and maintained at 80 °C for 6 h. Finally, the dark brown precipitate was washed with deionized water and dried to finally give the MnO_2/CNT .

Density functional theory calculations: The DFT calculation was carried out using DMol3 package. A double-numeric polarized basis set and all electron for the core-treatment were selected. For the numerical integration, the system was set as the open-shell (spin unrestricted) structure. The general gradient approximation with the Perdew-Burke-Ernzerh function (GGA-PBE) was applied for the electronic structure. The conductor-like screening model (COSMO) was used to simulate a H_2O solvent environment. The convergence tolerances of energy, maximum force and maximum displacement for structural optimization were 1.0×10^{-5} Ha, 0.002 Ha/Å and 0.005 Å, respectively. The self-consistent field (SCF) density convergence tolerance was 1×10^{-6} . The adsorption energy (E_{ads}) of the Zn^{2+} on B was defined as:

$$E_{\text{ads}} = E(\text{Zn}^{2+}/\text{B}) - E(\text{Zn}^{2+}) - E(\text{B})$$

where B represent the ZIL with functional groups. $E(\text{Zn}^{2+}/\text{B})$, $E(\text{Zn}^{2+})$ and $E(\text{B})$ were the energy of Zn^{2+} adsorbed on B, the energy of Zn^{2+} , and the energy of B, respectively.

Material Characterization: SEM images are observed by a JEOL JSM-7100F scanning electron microscope. X-ray diffractometer (XRD) with Cu K α radiation ($\lambda = 1.054056 \text{ \AA}$) with 2θ in the range of $5\sim 80^\circ$ are used to collect X-ray diffractometer characterizations. Fourier transform infrared Spectroscopy (FTIR) measurements were collected by using Nicolet 6700 (Thermo Fisher Scientific Co., USA). Atomic force microscope (AFM) images were conducted under tapping mode on a VEECO (Nanoscope IV/Nanoscope IV). The X-ray photoelectron spectroscopy (XPS) analysis was tested by ESCALAB 250 Xi spectrometer. The contact angles of the bare Zn, PAM-Zn, and PZIL-Zn were measured on Dataphysics OCA35 optical contact angle system for each test at the temperature of 25°C .

Electrochemical Measurements: The cathode slurry was prepared by mixing the MnO₂/CNT powder, acetylene black carbon, and PVDF in NMP solution at a weight ratio of 7:2:1. And then the slurry was coated onto a carbon paper. After drying, the carbon paper was cut into circular sheets. The areal mass loading of the cathode electrodes was about 1.3 mg cm^{-2} . All the electrochemical performances were tested with CR2016 coin cells assembled by a glass fiber separator. The Zn plating/stripping performance was measured in Zn||Zn (or PZIL-Zn||PZIL-Zn) symmetrical cells in 2 M ZnSO₄ solution. The CE of Zn anodes was measured with Zn||Cu (or Zn||PZIL-Cu) cells at a current density of 2 mA cm^{-2} for 0.5 h. The electrochemical performance of full cells (Zn||MnO₂ or PZIL-Zn||MnO₂) was tested at current density of 3 C in a voltage range of 0.9-1.8 V, using 2 M ZnSO₄ and 0.2 M MnSO₄ solution as electrolyte. All the

tests above were performed on a Neware Battery Tester. The EIS of the symmetrical cells in the frequency range of 0.01-100 kHz and CV curves of the full cells at a scan rate of 0.1 mV s^{-1} were tested by a BioLogic electrochemistry workstation.

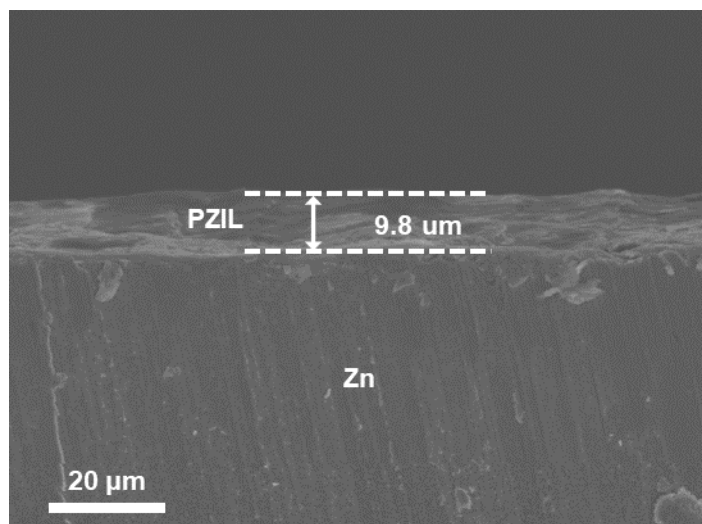


Figure S1. SEM cross section images of the decorated layer.

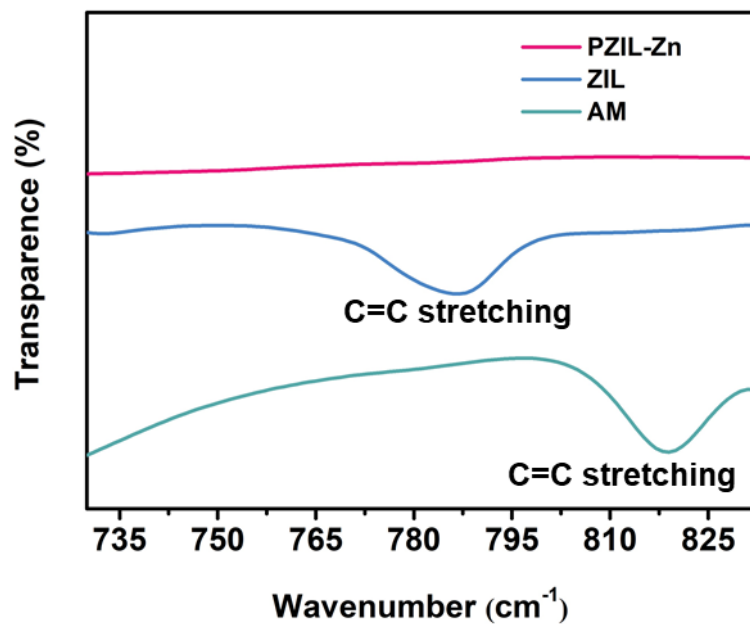


Figure S2. FTIR spectra of AM, ZIL, and PZIL-Zn. The IR peaks in the range of 780-830 cm⁻¹ are mainly ascribed to C=C twisting vibration. The characteristic peaks C=C bonds disappeared after polymerization.

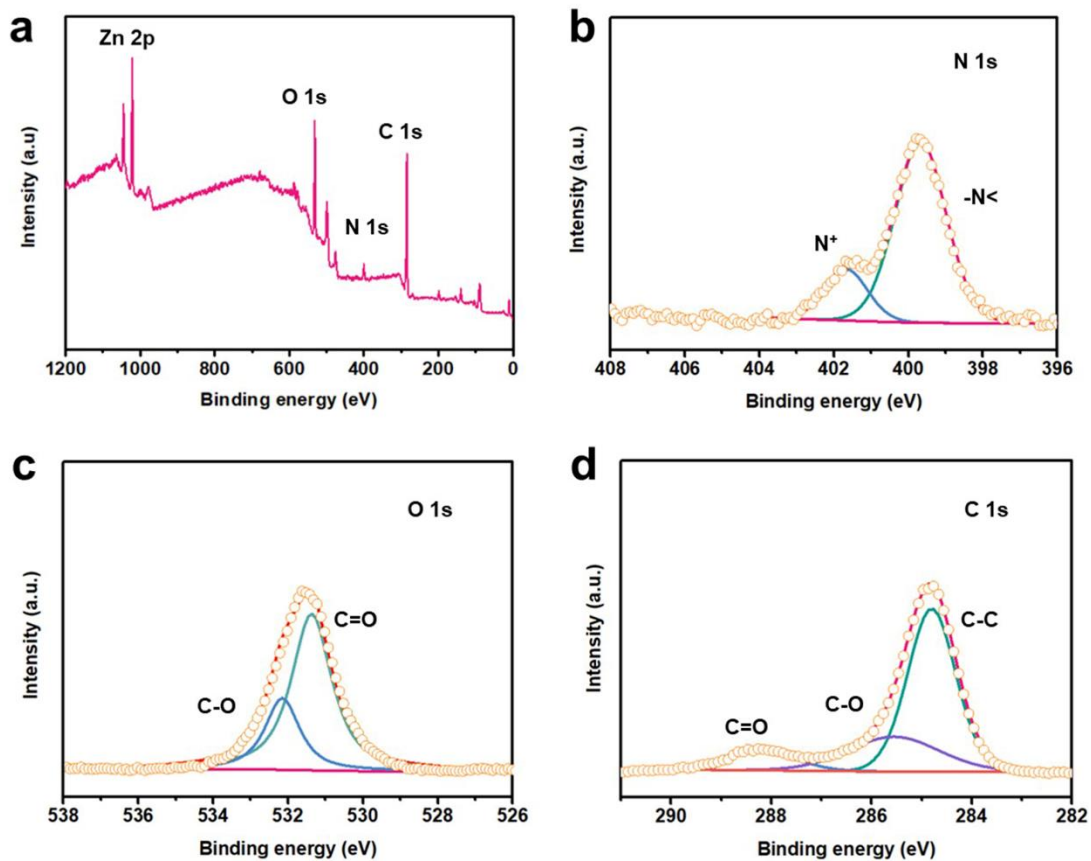


Figure S3. XPS spectrum of PZIL layer on Zn foil. (a) XPS survey scan of the PZIL-Zn. (b) High-resolution N 1s spectrum. (c) High-resolution O 1s spectrum. (d) High-resolution C 1s spectrum

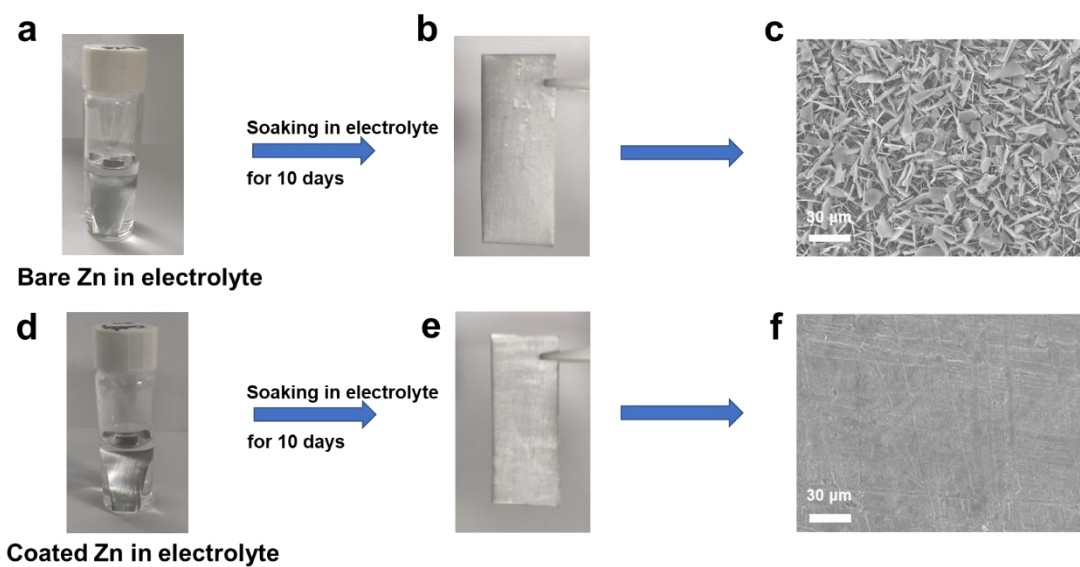


Figure S4. The stability of Zn and PZIL-Zn in 2 M ZnSO₄ electrolyte. (a,d) The bare Zn and PZIL-Zn soaked in electrolyte. (b,e) The optical image of soaked bare Zn and PZIL-Zn. (c,f) SEM images of soaked bare Zn and PZIL-Zn.

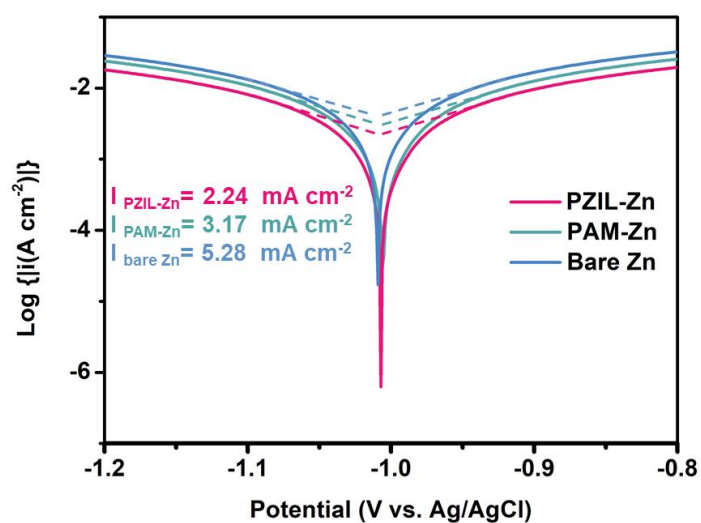


Figure S5. Linear polarization curves presenting the corrosion for bare Zn, PAM-Zn, and PZIL-Zn.

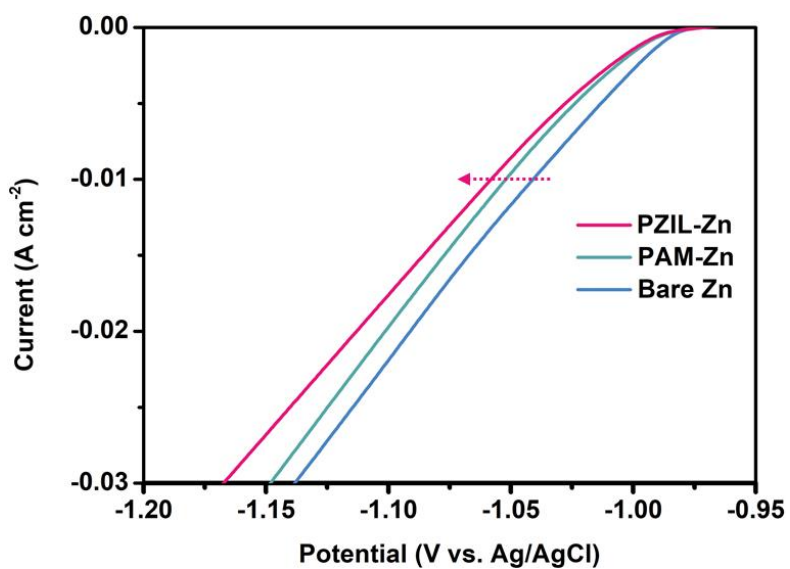


Figure S6. Corrosion curves of the bare Zn, PAM-Zn, and PZIL-Zn.

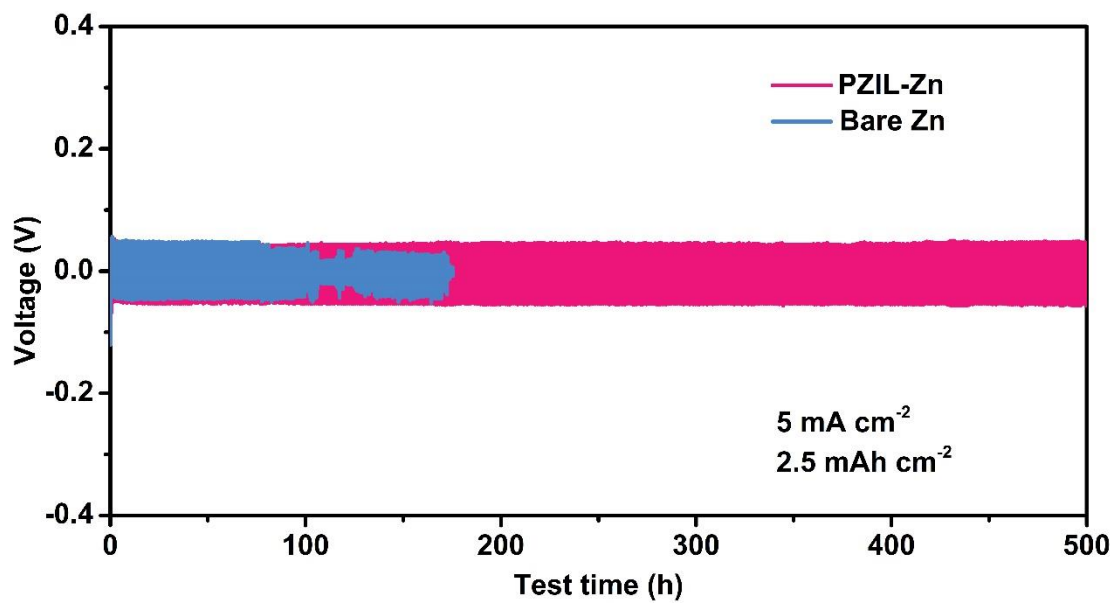


Figure S7. Zn plating/stripping performance for bare Zn metal and PZIL-Zn metal in the current density of 5 mA cm⁻².

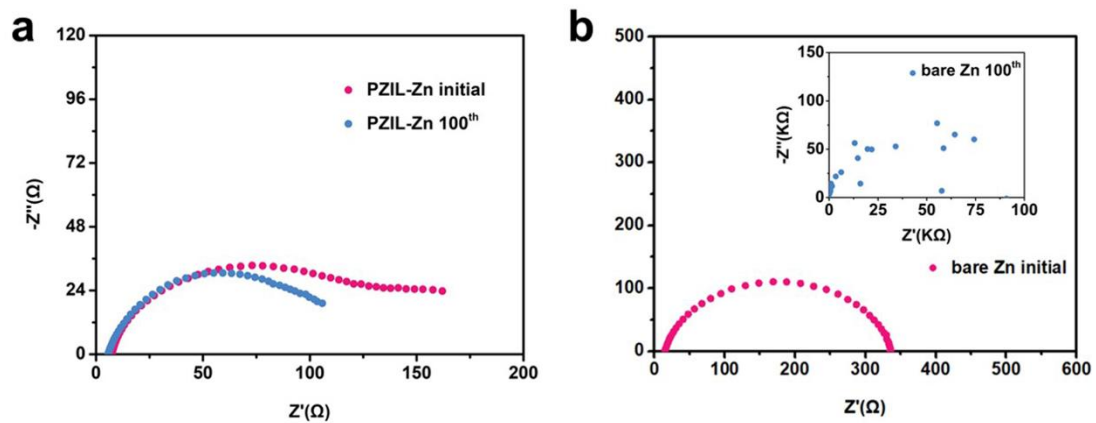


Figure S8. Nyquist plots of symmetric cells using (a) PZIL-Zn and (b) bare Zn before cycling and after 100 cycles.

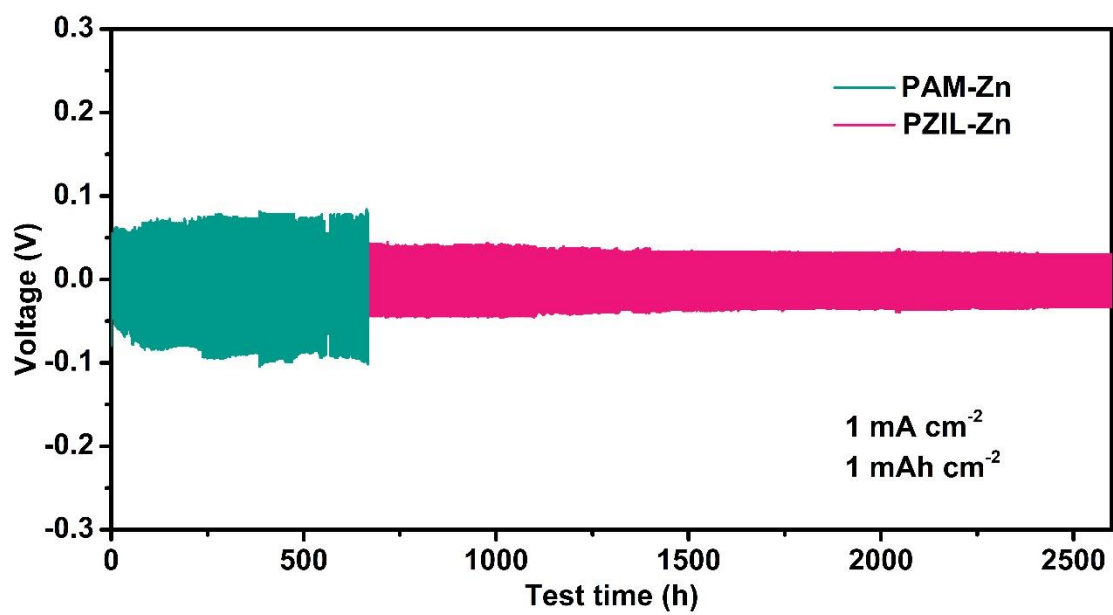


Figure S9. Zn plating/stripping performance for PAM-Zn and PZIL-Zn in the current density of 1 mA cm⁻².

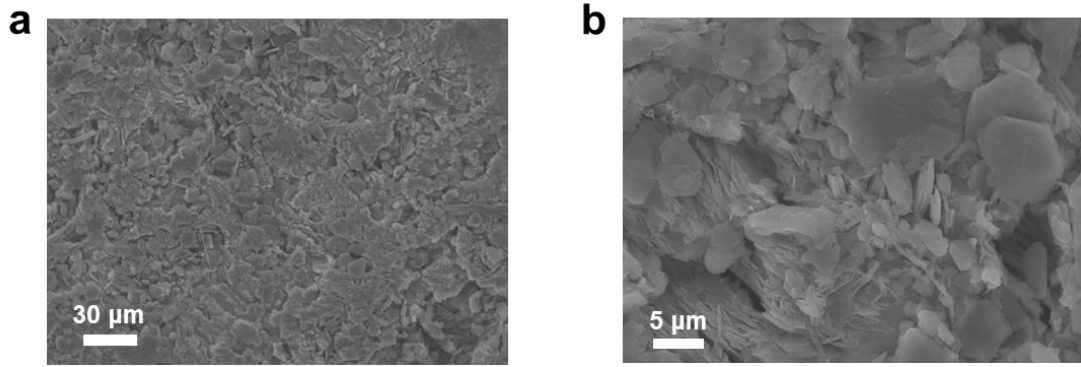


Figure S10. (a,b) SEM images of PAM-Zn after stripping/plating for 100 cycles at 1 mA cm^{-2} and 1 mAh cm^{-2} .

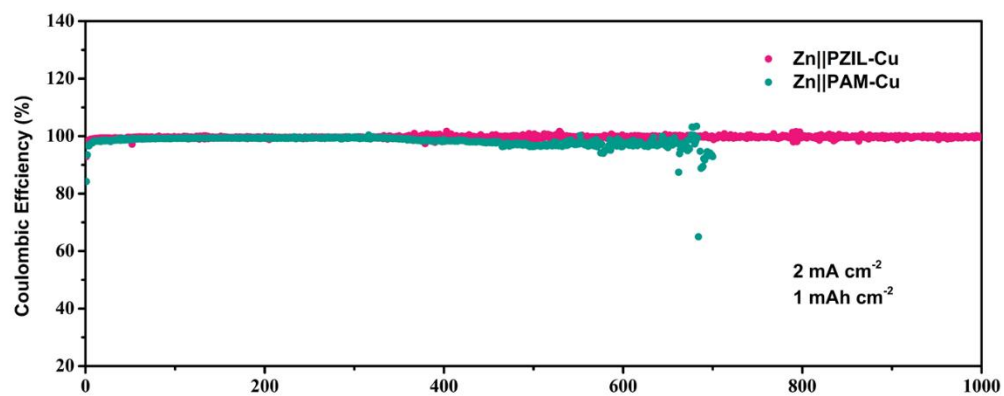


Figure S11. The CE tests of Zn||PZIL-Cu and Zn||PAM-Cu at a current density of 2 mA cm⁻².

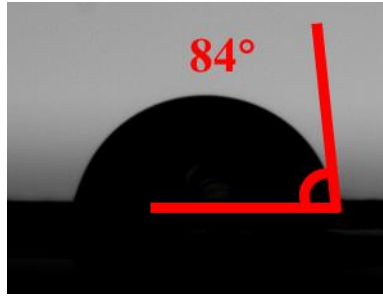


Figure S12. Static contact angle of 2 M ZnSO₄ electrolyte on PAM-Zn.

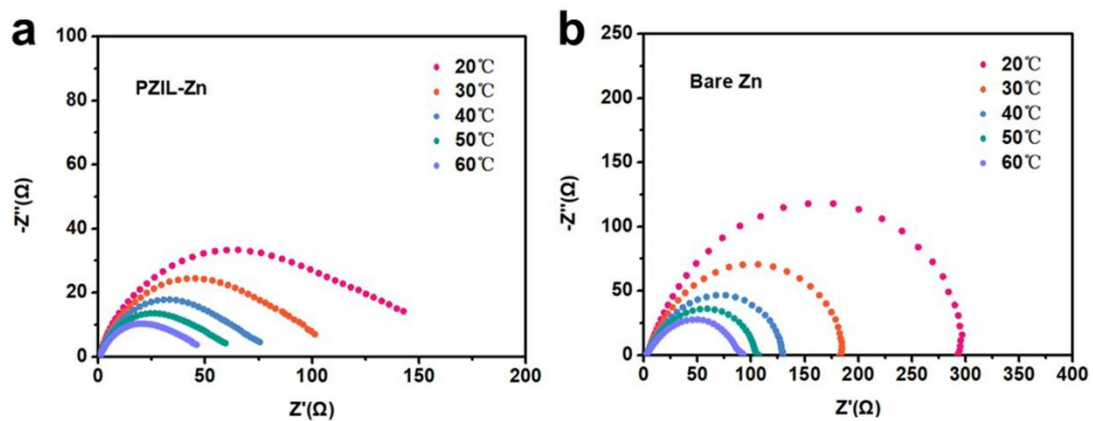


Figure S13. Nyquist patterns at different temperatures of the (a) bare Zn and (b) PZIL-Zn anode in symmetric cells.

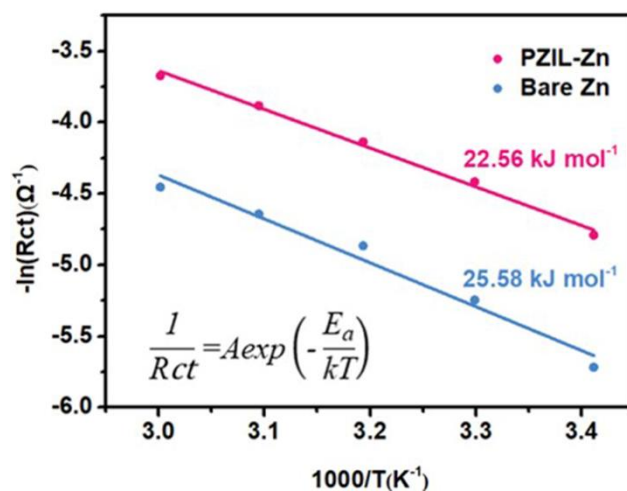


Figure S14. Arrhenius curves of bare Zn and PZIL-Zn anode.

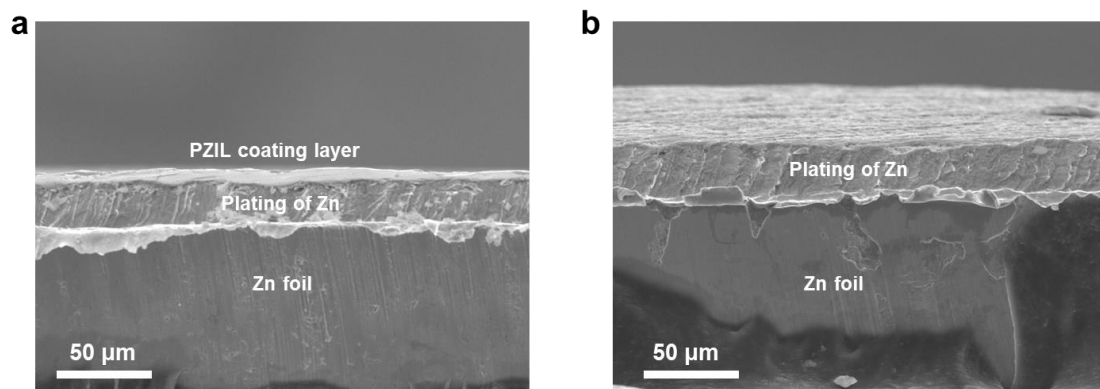
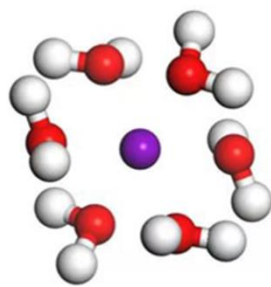


Figure S15. The cross-sectional SEM image of (a) cycled PZIL-Zn and (b) pull off the layer.



Ea = -9.59 eV

Figure S16. The calculated binding energies of Zn^{2+} with water.

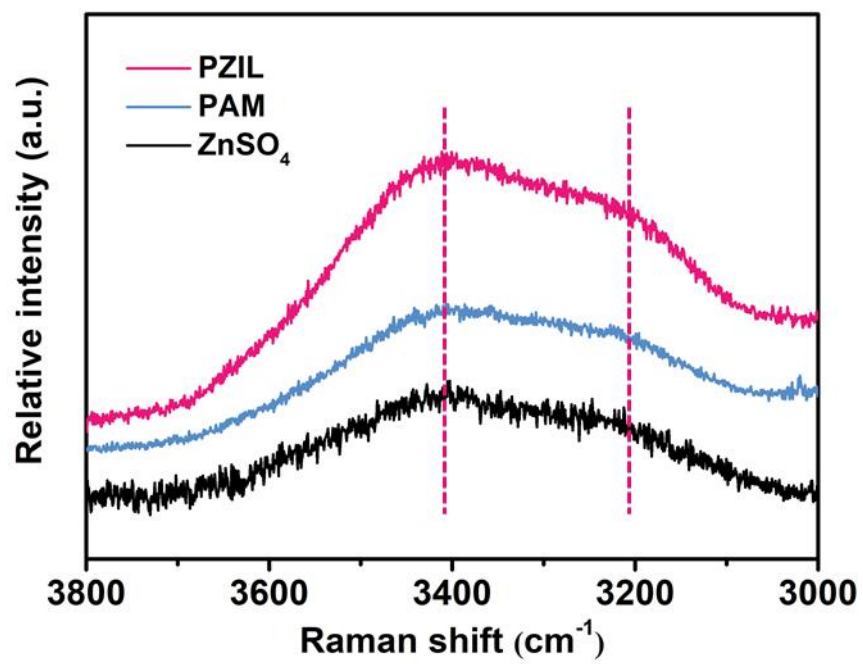


Figure S17. Intensity ratio of free water and bound water in Raman spectra.

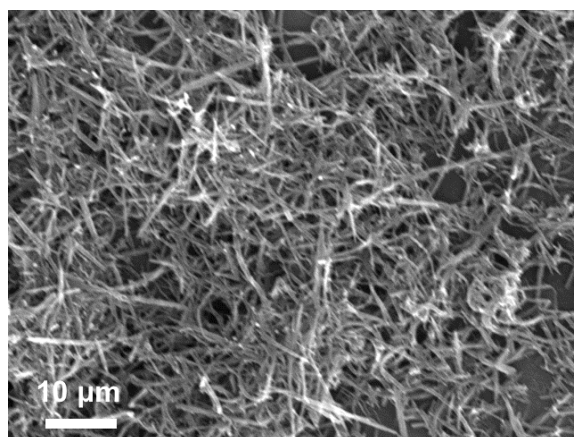


Figure S18. SEM image of the α -MnO₂/CNT composites.

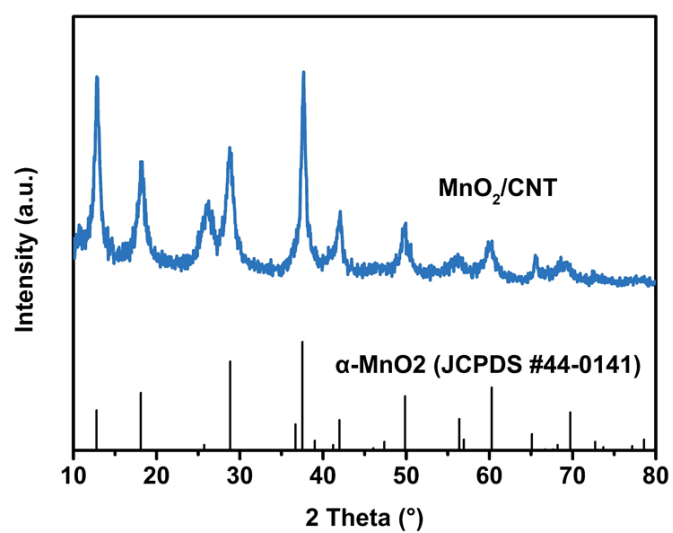


Figure S19. XRD pattern of the α -MnO₂/CNT composites.

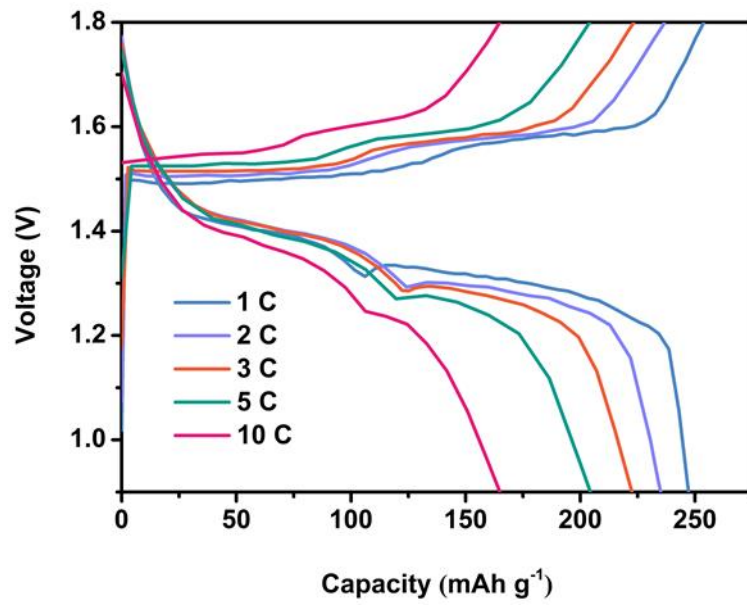


Figure S20. Charge/discharge curves of PZIL-Zn full cell at different current densities.

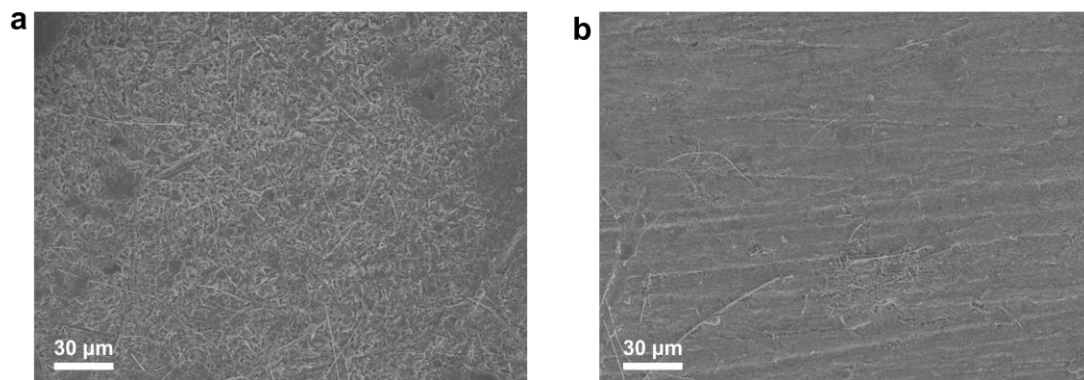


Figure S21. SEM images of the (a) surface of bare Zn and (b) PZIL-Zn full cell after 500 cycles.

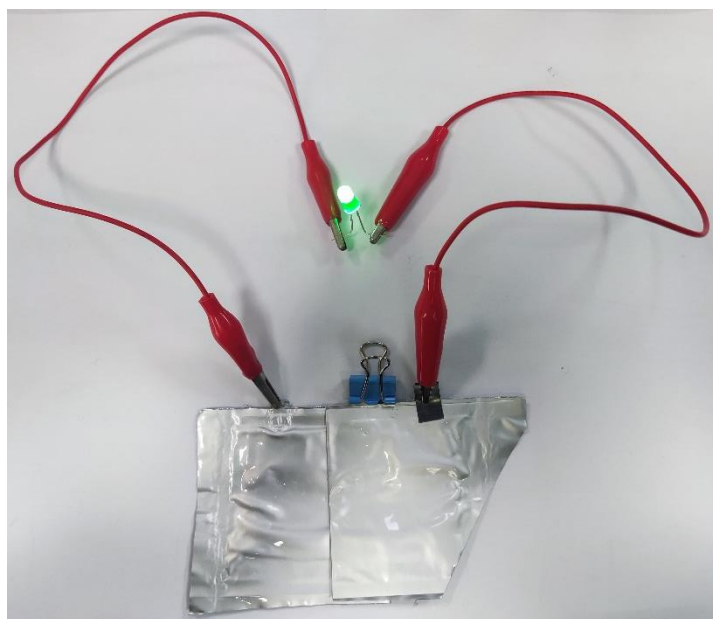


Figure S22. Digital photo of PZIL-Zn soft-packaged cells in series after being cut.

Table S1. Different zinc anode modification methods and the corresponding electrochemistry performance

Zinc anode	Current density (mA cm ⁻²)	Areal capacity (mAh cm ⁻²)	Worked time (h)	Reference
C@Zn (ZIF-8 pyrolysis)	1	1	400	3
PANZ@Zn	1	1	1145	4
MZn-60	0.2	0.2	800	5
In@Zn	0.25	0.05	1400	6
ZnO@Zn	5	1.25	500	7
Cu@Zn	1	0.5	1500	8
502@Zn	0.5	0.25	800	9
Pencil graphite@Zn	0.1	0.1	200	10
ZnS@Zn	2	2	1100	11
ZnF ₂ @Zn	1	1	800	12
Sc ₂ O ₃ @Zn	0.5	0.5	275	13
ALD-Al ₂ O ₃ @Zn	1	1	500	14
ZnF ₂ -rich SEI@Zn	0.1	0.05	1000	15
Faceted TiO ₂ @Zn	1	1	460	16
CM@CuO@Zn	1	1	400	17
In@Zn	1	1	500	18
PZIL@Zn	1	1	2600	This work

References for the Supporting Information

- (1) Liu, Z.; Wang, Y.; Ren, Y.; Jin, G.; Zhang, C.; Chen, W.; Yan, F. Poly(ionic liquid) hydrogel-based anti-freezing ionic skin for a soft robotic gripper. *Mater. Horizons* **2020**, *7* (3), 919-927.
- (2) Mo, F.; Liang, G.; Meng, Q.; Liu, Z.; Li, H.; Fan, J.; Zhi, C. A flexible rechargeable aqueous zinc manganese-dioxide battery working at -20 °C. *Energy Environ. Sci.* **2019**, *12* (2), 706-715.
- (3) Yuksel, R.; Buyukcakir, O.; Seong, W. K.; Ruoff, R. S. Metal - Organic Framework Integrated Anodes for Aqueous Zinc - Ion Batteries. *Adv. Energy Mater.* **2020**, *10* (16), 1904215.
- (4) Chen, P.; Yuan, X.; Xia, Y.; Zhang, Y.; Fu, L.; Liu, L.; Yu, N.; Huang, Q.; Wang, B.; Hu, X.; et al. An Artificial Polyacrylonitrile Coating Layer Confining Zinc Dendrite Growth for Highly Reversible Aqueous Zinc-Based Batteries. *Adv. Sci.* **2021**, *8* (11), e2100309.
- (5) Zhang, N.; Huang, S.; Yuan, Z.; Zhu, J.; Zhao, Z.; Niu, Z. Direct Self-Assembly of MXene on Zn Anodes for Dendrite-Free Aqueous Zinc-Ion Batteries. *Angew. Chem. Int. Ed.* **2021**, *60* (6), 2861-2865.
- (6) Hu, K.; Guan, X.; Lv, R.; Li, G.; Hu, Z.; Ren, L.; Wang, A.; Liu, X.; Luo, J. Stabilizing zinc metal anodes by artificial solid electrolyte interphase through a surface ion-exchanging strategy. *Chem. Eng. J.* **2020**, *396*, 125363.
- (7) Xie, X.; Liang, S.; Gao, J.; Guo, S.; Guo, J.; Wang, C.; Xu, G.; Wu, X.; Chen, G.; Zhou, J. Manipulating the ion-transfer kinetics and interface stability for high-performance zinc metal anodes. *Energy Environ. Sci.* **2020**, *13* (2), 503-510.
- (8) Cai, Z.; Ou, Y.; Wang, J.; Xiao, R.; Fu, L.; Yuan, Z.; Zhan, R.; Sun, Y. Chemically resistant Cu-Zn/Zn composite anode for long cycling aqueous batteries. *Energy Stor. Mater.* **2020**, *27*, 205-211.
- (9) Cao, Z.; Zhu, X.; Xu, D.; Dong, P.; Chee, M. O. L.; Li, X.; Zhu, K.; Ye, M.; Shen, J. Eliminating Zn dendrites by commercial cyanoacrylate adhesive for zinc ion battery. *Energy Stor. Mater.* **2021**, *36*, 132-138.
- (10) Li, Z.; Wu, L.; Dong, S.; Xu, T.; Li, S.; An, Y.; Jiang, J.; Zhang, X. Pencil Drawing Stable Interface for Reversible and Durable Aqueous Zinc - Ion Batteries. *Adv. Funct. Mater.* **2020**, *31* (4), 2006495.

- (11) Hao, J.; Li, B.; Li, X.; Zeng, X.; Zhang, S.; Yang, F.; Liu, S.; Li, D.; Wu, C.; Guo, Z. An In-Depth Study of Zn Metal Surface Chemistry for Advanced Aqueous Zn-Ion Batteries. *Adv. Mater.* **2020**, *32* (34), e2003021.
- (12) Yang, Y.; Liu, C.; Lv, Z.; Yang, H.; Zhang, Y.; Ye, M.; Chen, L.; Zhao, J.; Li, C. C. Synergistic Manipulation of Zn(2+) Ion Flux and Desolvation Effect Enabled by Anodic Growth of a 3D ZnF₂ Matrix for Long-Lifespan and Dendrite-Free Zn Metal Anodes. *Adv. Mater.* **2021**, *33* (11), e2007388.
- (13) Zhou, M.; Guo, S.; Fang, G.; Sun, H.; Cao, X.; Zhou, J.; Pan, A.; Liang, S. Suppressing by-product via stratified adsorption effect to assist highly reversible zinc anode in aqueous electrolyte. *J. Energy. Chem.* **2021**, *55*, 549-556.
- (14) He, H.; Tong, H.; Song, X.; Song, X.; Liu, J. Highly stable Zn metal anodes enabled by atomic layer deposited Al₂O₃ coating for aqueous zinc-ion batteries. *J. Mater. Chem. A* **2020**, *8* (16), 7836-7846.
- (15) Qiu, H.; Du, X.; Zhao, J.; Wang, Y.; Ju, J.; Chen, Z.; Hu, Z.; Yan, D.; Zhou, X.; Cui, G. Zinc anode-compatible in-situ solid electrolyte interphase via cation solvation modulation. *Nat. Commun.* **2019**, *10* (1), 5374.
- (16) Zhang, Q.; Luan, J.; Huang, X.; Wang, Q.; Sun, D.; Tang, Y.; Ji, X.; Wang, H. Revealing the role of crystal orientation of protective layers for stable zinc anode. *Nat. Commun.* **2020**, *11* (1), 3961.
- (17) Zhang, Q.; Luan, J.; Huang, X.; Zhu, L.; Tang, Y.; Ji, X.; Wang, H. Simultaneously Regulating the Ion Distribution and Electric Field to Achieve Dendrite-Free Zn Anode. *Small* **2020**, *16* (35), e2000929.
- (18) Han, D.; Wu, S.; Zhang, S.; Deng, Y.; Cui, C.; Zhang, L.; Long, Y.; Li, H.; Tao, Y.; Weng, Z.; Yang, Q.; Kang, F. A Corrosion-Resistant and Dendrite-Free Zinc Metal Anode in Aqueous Systems. *Small* **2020**, *16* (29), e2001736.